

## Article

# Significance of Temperature-Dependent Density on Dissipative and Reactive Flows of Nanofluid along Magnetically Driven Sheet and Applications in Machining and Lubrications

Zia Ullah <sup>1,\*</sup>, Ahmad Hussain <sup>2</sup>, Musaad S. Aldhabani <sup>3</sup>, Nifeen H. Altaweel <sup>3</sup> and Sana Shahab <sup>4</sup>

<sup>1</sup> Department of Mathematics and Statistics, The University of Lahore, Sargodha-Campus, Sargodha 40100, Pakistan

<sup>2</sup> Department of Physics, The University of Lahore, Sargodha 40100, Pakistan; ahmed\_00277@yahoo.com

<sup>3</sup> Department of Mathematics, Faculty of Science, University of Tabuk, P.O. Box 741, Tabuk 71491, Saudi Arabia; maldhabani@ut.edu.sa (M.S.A.); naltawil@ut.edu.sa (N.H.A.)

<sup>4</sup> Department of Business Administration, College of Business Administration, Princess Nourah bint Abdulrahman University, P.O. Box 84428, Riyadh 11671, Saudi Arabia; sshahab@pnu.edu.sa

\* Correspondence: ziakhan.uos.72@gmail.com

**Abstract:** Nanofluid lubrication and machining are challenging and significant tasks in manufacturing industries that are used to control the removal of a material from a surface by using a cutting tool. The introduction of a nanofluid to the cutting zone provides cooling, lubricating, and chip-cleaning benefits that improve machining productivity. A nanofluid is a cutting fluid that is able to remove excessive friction and heat generation. Chemical reactions and temperature-dependent density are essential in the thermal behavior of a nanofluid. The present study presents a careful inspection of the chemical reactions, temperature-dependent density, viscous dissipation, and thermophoresis during the heat and mass transfer of a nanofluid along a magnetically driven sheet. The physical attitude of viscous dissipation and the chemical reaction improvement rate in magneto-nanofluid flow is the primary focus of the present research. By applying the proper transformation, nonlinear partial differential expressions are introduced to the structure of the ordinary differential framework. The flow equations are simplified into nonlinear differential equations, and these equations are then computationally resolved via an efficient computational technique known as the Keller box technique. Flow factors like the Eckert number, reaction rate, density parameter, magnetic force parameter, thermophoretic number, buoyancy number, and Prandtl parameter governing the velocity, temperature distribution, and concentration distribution are evaluated prominently via tables and graphs. The novelty of the current study is in computing a heat transfer assessment of the magneto-nanofluid flow with chemical reactions and temperature-dependent density to remove excessive friction and heating in cutting zones. Nanofluids play significant roles in minimum quantity lubrication (MQL), enhanced oil recovery (EOR), drilling, brake oil, engine oil, water-miscible cutting fluids, cryogenic cutting fluids, controlled friction between tools and chips and tools and work, and conventional flood cooling during machining processes.

**Keywords:** viscous dissipation; temperature-dependent density; reactive flow; nanofluid; lubrications; machining; heat transfer; magnetically driven sheet



**Citation:** Ullah, Z.; Hussain, A.; Aldhabani, M.S.; Altaweel, N.H.; Shahab, S. Significance of Temperature-Dependent Density on Dissipative and Reactive Flows of Nanofluid along Magnetically Driven Sheet and Applications in Machining and Lubrications. *Lubricants* **2023**, *11*, 410. <https://doi.org/10.3390/lubricants11090410>

Received: 10 August 2023

Revised: 11 September 2023

Accepted: 12 September 2023

Published: 18 September 2023



**Copyright:** © 2023 by the authors. Licensee MDPI, Basel, Switzerland. This article is an open access article distributed under the terms and conditions of the Creative Commons Attribution (CC BY) license (<https://creativecommons.org/licenses/by/4.0/>).

## 1. Introduction and Literature Review

Nanofluids were initially created to improve the performance of minimum quantity lubrication (MQL) and overflow cooling. The particles of manufactured nanomaterials suspended in base fluids are known as nanofluids. MQL is the greatest choice as a base fluid for nanotechnologies because this fluid is currently popular for its high efficiency compared to traditional overflow cooling fluids. The idea of nanofluid lubrication was established as a result of developing nanotechnologies. Using nanofluid substituting for

frequently employed cutting fluids, a procedure known as nano-lubrication, can efficiently cool and lubricate cutting regions during manufacturing operations. A substance's specified dimension, shape, and surface polish are obtained with the elimination of additional substances in the form of tiny pieces during cutting, which is now thought to be the best possible mechanical technique. The results of the present research can improve our awareness of nanofluid EOR procedures through the angle of oil-based substances, nanoparticles, and interfacial dynamics. They can also help us to figure out how nanofluids perform in multiphase fundamental movement modeling and assessments. For the majority of machining tools, an increased efficiency is anticipated to be mostly based on the significantly and substantially strong temperature-sensitive thermal conduction of nanofluids. Cutting tools are required to eliminate additional substances by making direct frictional contact. Due to its significance across multiple manufacturing and scientific procedures, including liquid film vaporization, the aerodynamic protrusion of polymeric spreadsheets, the formation of crystals, the cooling of solid papers, the design of manufacturing instruments and several heat exchange systems, and glass and polymeric sectors, the examination of the flow within a drastically stretched sheet is of significant importance. Khan et al. [1] used computational methods to examine the effects of solar radiation, heat production, and chemical processes on a stationary flow separation through a wedge-like structure in electromagnetic water. Magneto-nanofluid motion caused by an elongated surface was discussed by Anjum et al. [2]. In the context of chemical reactions and radiation temperature factors, a researcher [3] explored the magnetic flow separation of tiny liquids and heat transmission through a dynamic stretchable surface. Zhang et al. [4] looked at the impacts of a plant-based oil's thickness, friction, and molecular composition on its ability to cool and its lubricated qualities. The radiative heat transmission of nanofluids across a wedge-shaped structure that is receptive to initial-order chemical reactions, temperature generation absorption, and vacuum forces was investigated by Kasmani et al. [5]. Doshi et al. [6] discussed the difficulties involved in using a nanofluid as a cutting fluid for machine work. The impact of Darcy's homogenous chemical processes on higher-order nanofluids was examined by Jagadha et al. [7].

During either the initial or subsequent oil extraction operations, reserved oil can often be recovered via enhanced oil recovery (EOR). Chemical EOR has shown to achieve excessive oil extraction with minimal operating expenses when compared with traditional techniques, and nanofluids have drawn a lot of interest due to their beneficial characteristics of affordability, excessive oil extraction, and broad applicability. Additionally, a number of research findings have concentrated on the function of nanoparticles in the nanofluid EOR procedure. The wetting capability of materials (surface/particle micromechanics), the stiffness at the water–oil interface (massive fuel/molecule micromechanics), and the stress at the mechanically disjoining interface (heavy fuel/molecules/particle micromechanics) can all be affected by nanofluids. Moreover, they may reduce thickness (micromechanics of massive oil nanoparticles). Furthermore, nanomaterials are capable of sticking to the surfaces of water and oil, changing the surface tension and causing an emulsion to develop. Rao et al. [8] calculated the rates of heat transmission for a basic liquid and a mixture with nanoscale integration, and an analysis of finite elements was used to generate the heating ranges of a cutting instrument. Afify [9] quantitatively explored the effects of numerous slips with viscosity dissipations on the flow separation and heat transmission of unconventional nanoparticles across an extensible sheet. Hasin et al. [10] combined several different kinds of nanomaterials with a supporting liquid to enhance the machining and cutting abilities of ordinary plant-based oil. Srikant et al. [11] looked into various methods to substitute the deployment of cutting liquids for minimal lubrication. The significance of nanotechnology in machining procedures was studied by Kadirgama [12]. The topic was covered in many sections, including the cutter effect, the roughness on the surface, tool durability, and tool corrosion.

The use of injecting liquids, nano-foam engineering, and nano-emulsion manufacturing is crucial for the enhanced oil recovery (EOR) procedure. The nanoparticle absorbing

reaction serves as the foundation for the nanofluid EOR system. When a nanomaterial attaches to a metallic substrate, the wetness of the material changes from a remaining oil-wet state to moist with water. Additionally, a nanomaterial is capable of attaching to the outermost layers of water and oil, changing the surface tension and causing emulsions to develop. There is a greater need for brake devices with better and more effective thermal dissipation methods and characteristics to decrease drag forces to enhance automotive aerodynamic efficiency. Nanofluids are crucial for minimizing resistance and maximizing the transmission of heat to resolve this problem. The current mechanism is crucial for dual-phase flows, thermal exchange optimized performance, fuel cell development, and geothermal power installations. Entropy formation in a streaming liquid has been the topic of many investigations in the field of science. Li and Ali [13] provided a thorough discussion of the many facets of nanofluids, including their characterization, movement, and energy transfer procedures. The approaches for characterizing the several characteristics of nanofluids, such as their thermal conductivity and the variables affecting it, were presented. Sharma et al. [14] summarized several significant peer-reviewed papers on the use of nanofluids in cutting, tapping, crushing, and spinning operations. To improve thermal and heat transmission, a nanofluid is used as a cutting fluid in machining. For enhancing efficiency, micro-lubrication methods and method modification play similar roles [15]. During machining, manufacturing heat is an essential occurrence. Rifat et al. [16] employed various cooling systems and tool durability to eliminate the heat-related negative consequences of skin burning. Sidik et al. [17] discussed the most current development and uses of nanofluids in machining operations. They reviewed numerous traditional and modern cooling strategies used in machining and to improve thermal conductivity and studied the characteristics of nanofluids. Amin et al. [18] examined the impact of nanofluid flow behavior in machining procedures. An experimental study on the effectiveness of environmentally friendly plant-based oil nanofluids in rotating movement was conducted by Pasam et al. [19]. During machining, the cutting levels, cutting pressures, tool wear, and surface roughness were determined for stable cutting circumstances. For all interatomic connections, Lautenschlaeger [20] employed the Lennard-Jones shortened and shifting formulation. For the accuracy and justification of results, the numerical outcomes of heat transfer were compared with the existing literature in [21–23]. The effects of temperature-dependent density or variable density on the heat transfer assessment of viscous and nanofluid flow along various geometries was reported in [24–40] and published in well-reputed journals. Dolatabadi et al. [41] performed a heat transfer improvement of engine oil by assuming the temperature-dependent viscosity.

The originality of the current work is to resolve problems in high-temperature systems. Most studies are found to deal with a small temperature difference between the surface and ambient nanofluid. However, circumstances arise where this temperature difference is high. In this situation, the density is assumed as an exponential function of temperature, and the nanofluid is assumed to be electrically conducting in the sense of ionized nanofluid due to the high operating temperature. The nanofluid density is assumed to be reduced exponentially with temperature and the relation for this mechanism. The magnetic field is applied on the surface to decrease excessive heat through tool chips and tool works during the machining procedure in the cutting region. The nanofluid works as a cutting fluid to lubricate the surface to prevent extreme temperatures. The introduction of an electrically conducting nanofluid to the cutting zone provides cooling, lubricating, and chip-cleaning benefits that improve machining productivity. Several scientists explored the temperature-dependent density flows in various fluid geometries ([2,3,9,24–40]). The novelty of the present analysis is to produce cooling in cutting tools in the presence of nanofluid lubrication. The impact of a chemical reaction, viscous dissipation, and temperature-dependent density on a magneto nanofluid along a stretching surface is explored. The thermal and concentration boundary layer of a nanofluid is examined along a stretching sheet numerically. The present work is original and significant because it

satisfies the given boundary conditions. For the originality of the current research, the numerical findings of the heat and mass transfer are compared with the published research.

## 2. Mathematical Formulation and Flow Shape

The research topic is based on a computational analysis of the effects of variable density, chemical reaction, and viscous dissipation on the heat transfer and nanoparticle characteristics of a nanofluid over a stretching sheet under thermophoretic and Brownian motion. The current problem is converted into a set of partially differentiated conditions through stream-function modifications and then transformed into an ordinary form. The constructed problem is resolved through the integration of the Keller box technique with the finite difference method (FDM) procedure. The logical outcomes for the physical characteristics under consideration will be represented visually and in tabulated form.

Consider the potentially magnetically driven two-dimensional nanomaterial shown in Figure 1, where  $u$  and  $v$  define the velocity distributions in  $x$  and  $y$  directions, respectively. The axes  $x$  and  $y$  are the directions along the surface and normal to the stretching surface. The temperature is expressed by  $T$ , the stream-free temperature is denoted by  $T_\infty$ , the fluid thermal conductivity is indicated by  $\kappa$ , and the particular heat is expressed by  $C_p$ . The thickness is marked by  $\rho$ , the density of the particles is marked by  $\rho_p$ , the kinematics viscosity of the fluid is marked by  $\nu = \mu/\rho$ , the acceleration due to gravitation is marked by  $g$ , and the fluid density is marked by  $\rho_f$ . The mathematical models for the electromagnetic force, momentum, energy, and continuum are as follows [1–3]:

$$\frac{\partial(\rho u)}{\partial x} + \frac{\partial(\rho v)}{\partial y} = 0 \quad (1)$$

$$u \frac{\partial u}{\partial x} + v \frac{\partial u}{\partial y} = -\frac{1}{\rho} \frac{\partial p}{\partial x} + \frac{\mu}{\rho} \frac{\partial^2 u}{\partial y^2} - \frac{\sigma^* B_0^2 u}{\rho} + \frac{g}{\rho} (\rho_\infty - \rho) \quad (2)$$

$$u \frac{\partial v}{\partial x} + v \frac{\partial v}{\partial y} = -\frac{1}{\rho} \frac{\partial p}{\partial y} + \frac{\mu}{\rho} \frac{\partial^2 v}{\partial y^2} - \frac{\sigma^* B_0^2 v}{\rho} + \frac{g}{\rho} (\rho_\infty - \rho) \quad (3)$$

$$u \frac{\partial T}{\partial x} + v \frac{\partial T}{\partial y} = \frac{\kappa}{(\rho c_p)_f} \frac{\partial^2 T}{\partial y^2} + \frac{(\rho c_p)_p}{(\rho c_p)_f} \left\{ D_B \frac{\partial C}{\partial y} \frac{\partial T}{\partial y} + \left( \frac{D_T}{T_\infty} \right) \left( \frac{\partial T}{\partial y} \right)^2 \right\} + \frac{\nu}{(\rho c_p)_f} \left( \frac{\partial u}{\partial y} \right)^2 \quad (4)$$

$$u \frac{\partial C}{\partial x} + v \frac{\partial C}{\partial y} = D_B \frac{\partial^2 C}{\partial y^2} + \left( \frac{D_T}{T_\infty} \right) \frac{\partial^2 T}{\partial y^2} - k_r (C - C_\infty) \quad (5)$$

The boundary conditions of the current methodology are

$$v = 0, \quad u = u_w(x) = ax, \quad T = T_w, \quad C = C_w \quad \text{at} \quad y = 0 \quad (6)$$

$$u = v \rightarrow 0, \quad T \rightarrow T_\infty, \quad C \rightarrow C_\infty \quad \text{as} \quad y \rightarrow \infty.$$

The required boundary parameters for both the temperature and elements of velocity are described in the section above.  $P$  signifies pressure,  $\rho$  is for the base fluid density,  $\alpha$  is for the heating diffusion,  $\nu$  is for the kinematic viscosity,  $a$  is for a certain constant,  $D_B$  is for the Brownian distribution,  $D_T$  is for the thermophoretic distribution, and  $\tau = (\rho c)_p / (\rho c)_f$  is for the proportion of the efficient heat ability of the nanoparticle substance to the fluid heat ability, where  $\rho$  appears for density and  $c$  is for the factor of heat conductance.

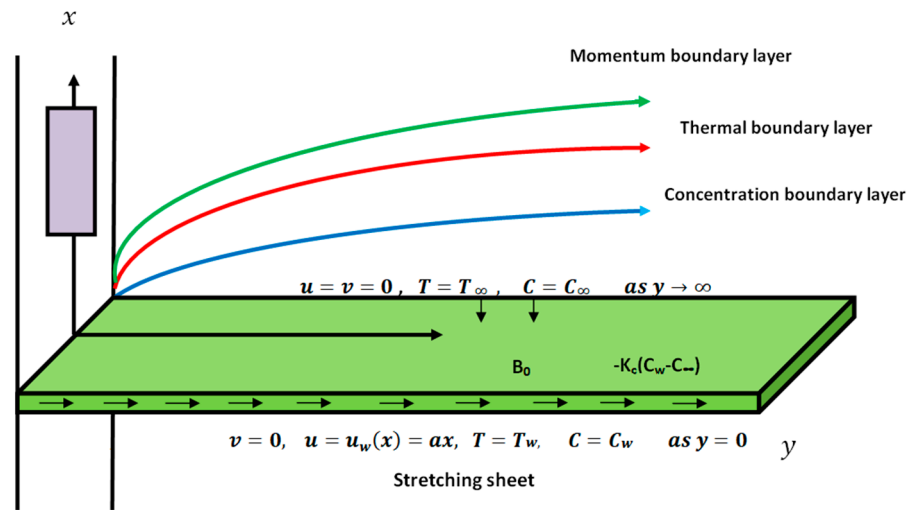


Figure 1. Geometrical sheet with flow behavior.

### 3. Stream Factors and Similarity Analysis

The stream factors and similarity factors for the conversion of partial equations into ordinary equations are expressed below [5,7,9].

$$u = \frac{1}{\rho} \frac{\partial \psi}{\partial y}, \quad v = -\frac{1}{\rho} \frac{\partial \psi}{\partial x}, \quad \phi(\eta) = \frac{C - C_\infty}{C_w - C_\infty} \quad p = p_o(\text{constant}) \quad (7)$$

The stream factors for concentration, velocity, and temperature distribution are expressed below.

$$\psi = (av)^{\frac{1}{2}} x f(\eta), \quad \theta(\eta) = \frac{T - T_\infty}{T_w - T_\infty}, \quad \eta = (a/v)^{1/2} y \quad (8)$$

The convenient terms of the modified ordinary equations are evaluated in Equations (9)–(11).

$$(f'^2 - f f'') = e^{-n\theta} (f''' - n\theta' f'') - e^{n\theta} \zeta f' - \lambda \left( \frac{1 - e^{n\theta}}{1 - e^{-n}} \right) \quad (9)$$

$$\frac{e^{-n\theta}}{Pr} (\theta'' - n\theta'^2) + f\theta' + (e^{-n\theta})^2 [N_B \phi' \theta' + N_T \theta'^2] + (e^{-n\theta})^2 Ec (f'')^2 = 0 \quad (10)$$

$$(e^{-n\theta})^2 [(\phi'' - n\phi' \theta') + Le \frac{N_T}{N_B} (\theta'' - n\theta'^2)] + Le (f\phi' - \sigma\phi) = 0 \quad (11)$$

Here,  $Ec = \frac{U^2}{C_p \Delta T} = \frac{a^2 x^2}{C_p (T_w - T_\infty)}$  is described as the Eckert number,  $N_T = \frac{(\rho c)_p D_T (T_w - T_\infty)}{(\rho c)_f v T_\infty}$  is addressed as the thermophoresis parameter,  $\zeta = \frac{\sigma^* B_0^2 x}{\rho a}$  is designated as the magneto force parameter,  $N_B = \frac{(\rho c)_p D_B (\phi_w - \phi_\infty)}{(\rho c)_f v}$  is designated as the Brownian parameter,  $\theta$  is represented as the non-dimensional temperature,  $Le = \frac{v}{D_B}$  is defined as the Lewis parameter,  $\eta$  is indicated as the similarity factor,  $Pr = \frac{\nu}{\alpha}$  is denoted as the Prandtl number,  $\sigma = \frac{k_r^2}{a}$  is the reaction rate, and  $\nu = \frac{\mu}{\rho}$  is denoted as the kinematical viscosity. The appropriate boundary values are described in Equation (12).

$$f(0) = 0, \quad f'(0) = 1, \quad \theta(0) = 1, \quad \phi(0) = 1 \quad \text{at } \eta = 0 \quad (12)$$

$$f'(\infty) = 0, \quad \theta(\infty) = 0, \quad \phi(\infty) = 0 \quad \text{at } \eta \rightarrow \infty.$$

#### 4. Numerical Procedure and Method

The nonlinear ordinary differentiated form is reduced in the algebraic system of equations by offering the Keller box method (KBM) under defined boundaries. For smooth coding through MATLAB, the Newton–Raphson Scheme (NRC) is applied to alter the system of Equations (9)–(12) in the matrix notation.

$$A\delta = r \quad (13)$$

$$[A] = \begin{bmatrix} ([A_1][C_1]) & \dots & \dots \\ ([B_2][A_2][C_2]) & \ddots & \vdots \\ \vdots & \dots & ([B_{n-1}][A_{n-1}][C_{n-1}]) \\ \vdots & \dots & ([B_n][A_n]) \end{bmatrix}, \quad [\delta] = \begin{bmatrix} [\delta_1] \\ [\delta_2] \\ \vdots \\ [\delta_{n-1}] \\ [\delta_n] \end{bmatrix}, \quad [r] = \begin{bmatrix} [r_1] \\ [r_2] \\ \vdots \\ [r_{n-1}] \\ [r_n] \end{bmatrix} \quad (14)$$

#### 5. Results and Discussion

The relationship between the chemical reaction, heat density, and viscous dissipation in a laminar, two-dimensional, mixed convective flow of a magneto nanofluid over a stretching sheet is shown in the present investigation. The fluid density is assumed as an exponential component of temperature in the current model. By using the variable density, the solutions are valid across any significant temperature variation. The boundary layer equations are developed for the present mechanism under defined boundary conditions. It is important to note that the dimensionless governing mathematical equations are additionally simplified to a group of non-similar calculations with the support of the stream function structure and are numerically incorporated through the Keller box approach to compare the findings with those of previous investigations. The numerical findings from this technique are discussed above geometrically with acceptable agreement. The governing flow factors like the Eckert number, density parameter, magnetic force parameter, thermophoretic number, buoyancy number, and Prandtl parameter on the velocity, temperature distribution, and concentration distribution are evaluated prominently via tables and graphs.

The impact of the reaction rate  $\sigma$  on the velocity, temperature distribution, and concentration distribution is depicted in Figure 2a–c. The velocity graph increases as the reaction rate increases with good variations. Similarly, the temperature attains maximum magnitude as the reaction rate increases in the presence of entropy generation. The mass distribution decreases as the reaction rate decreases. The prominent variations in each plot are noted. The consequences of the thermal density parameter  $n$  on the velocity, temperature distribution, and concentration distribution are plotted in Figure 3a–c in the presence of entropy generation. The prominent variations in the velocity distribution are examined for each  $n$ . The velocity of a water-based fluid increases for a lower density but decreases as  $n$  increases. The certain amplitude in the temperature distribution is illustrated as  $n = 0$  but decreases as the density parameter increases. Similarly, the concentration distribution increases as the density of fluid decreases for  $Pr = 7.0$ . The minimum concentration is evaluated for the maximum density in the presence of entropy generation. Physically, the buoyant pressure increases for higher values of the density factor, which leads to growth density variations with temperatures. In Figure 4a, the impact of the Eckert number  $Ec$  on the velocity distribution yields an enhancement with feasible asymptotic behavior with  $n = 0.4$ . The temperature of the water-based fluid increases as the Eckert number increases with prominent variations in Figure 4b. Physically, it is valid because the entropy generation acts like a heat source to produce the ability in the temperature of the fluid. The concentration  $\phi$  is increased for a lower entropy generation and decreases as the Eckert number is enhanced in Figure 4c. It can be observed that each physical profile yields prominent variations. The influence of the Prandtl number on the velocity distribution, concentration, and temperature distribution is evaluated in Figure 5a–c for  $Pr = 0.7, 1.0, 3.0, 5.0,$  and  $7.0$  with some fixed quantities. The Prandtl number has a significant impact on the flow rate

through the plotted profiles. The velocity of the fluid boosts for a lower Pr and gradually decreases as the Pr increases. The prominent enhancement in the temperature of the fluid is assessed for the maximum Pr but decreases as the Pr decreases. Moreover, a reasonable change in the concentration distribution is evaluated for each Pr with entropy generation. According to scientific logic, this is valid because the entropy growth significantly boosts the thermal energy of the fluid, which increases the fluid’s temperature. Additionally, the influence of the magneto force  $\zeta$  is drafted in Figure 6a–c with the entropy generation and density variations. It is assessed that the velocity of the fluid and temperature decreases as  $\zeta$  increases. The prominent enhancements in both the temperature and velocity are depicted for lower values of  $\zeta$ . On the other hand, the concentration distribution enhances as  $\zeta$  is reduced. It is normally understood because a boost in the Prandtl value causes a reduction in the fluid’s thermal conduction, which, in turn, reduces the amount of frictional force within the viscosity layers. The numerical results of the velocity  $f'(\eta)$ , temperature  $\theta$ , and concentration  $\phi$  are drafted in Figure 7a–c for various choices of the Brownian motion  $Nb$  under the impacts of viscous dissipation and the magnetic field across the stretched sheet for a high temperature difference.

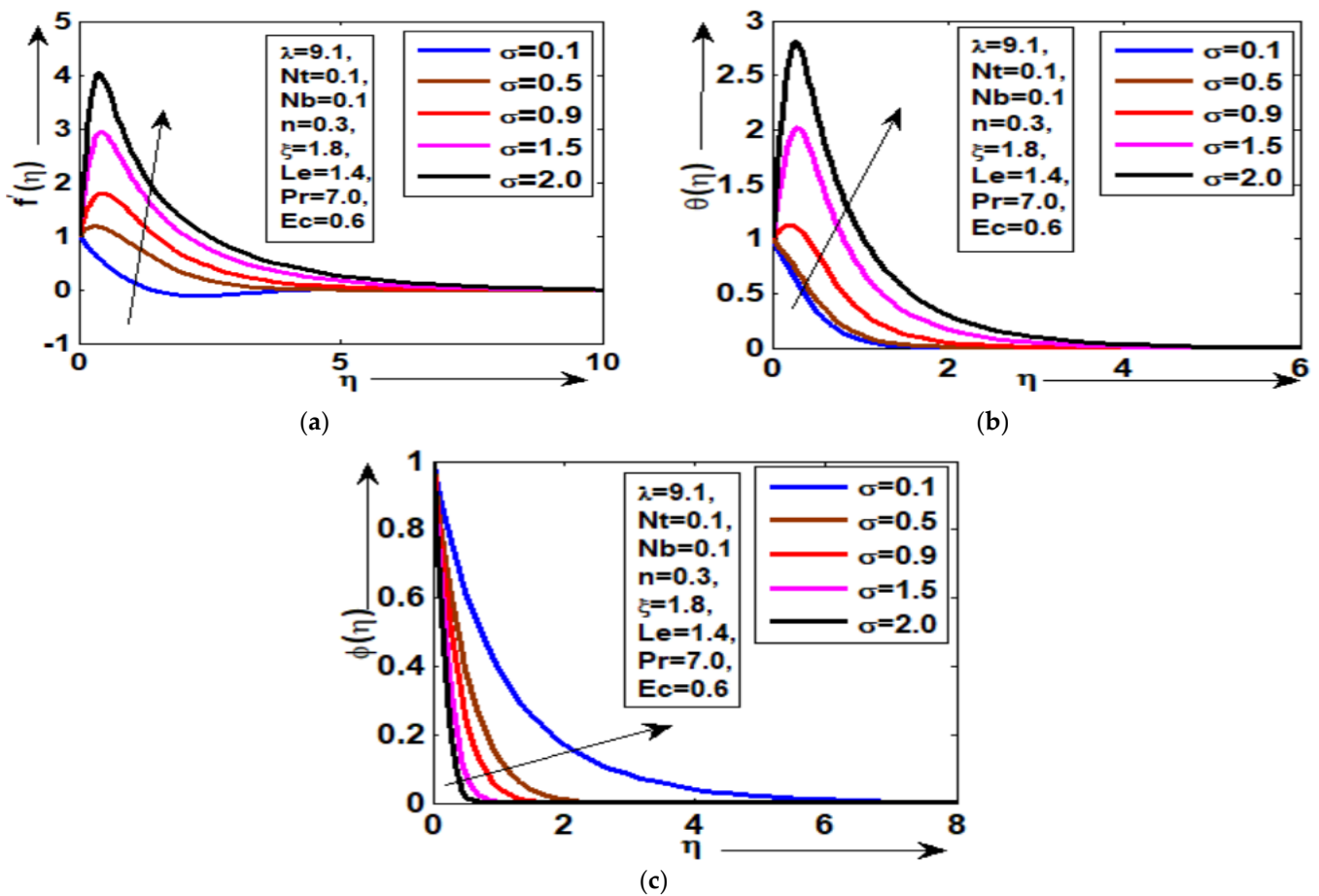


Figure 2. (a–c) Graphical behavior of velocity  $f'(\eta)$ , temperature  $\theta(\eta)$  and concentration  $\phi(\eta)$  for  $\sigma$ .

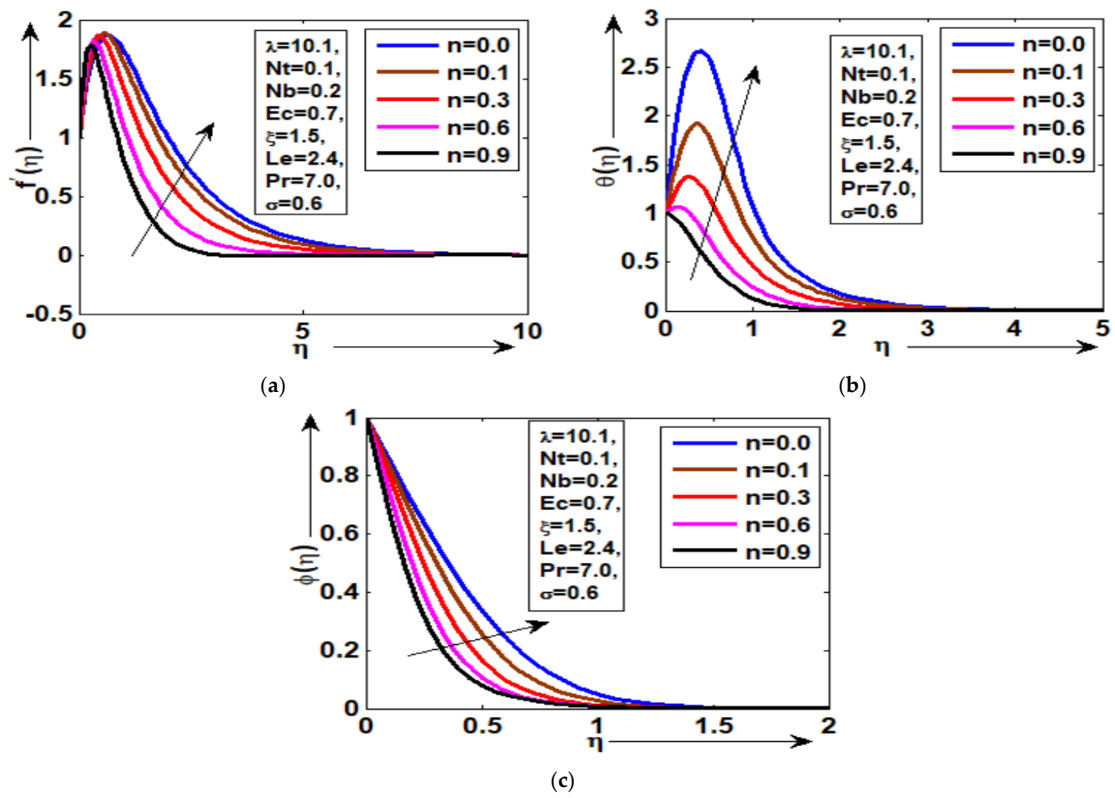


Figure 3. (a–c) Graphical behavior of velocity  $f'(\eta)$ , temperature  $\theta(\eta)$  and concentration  $\phi(\eta)$  for  $n$ .

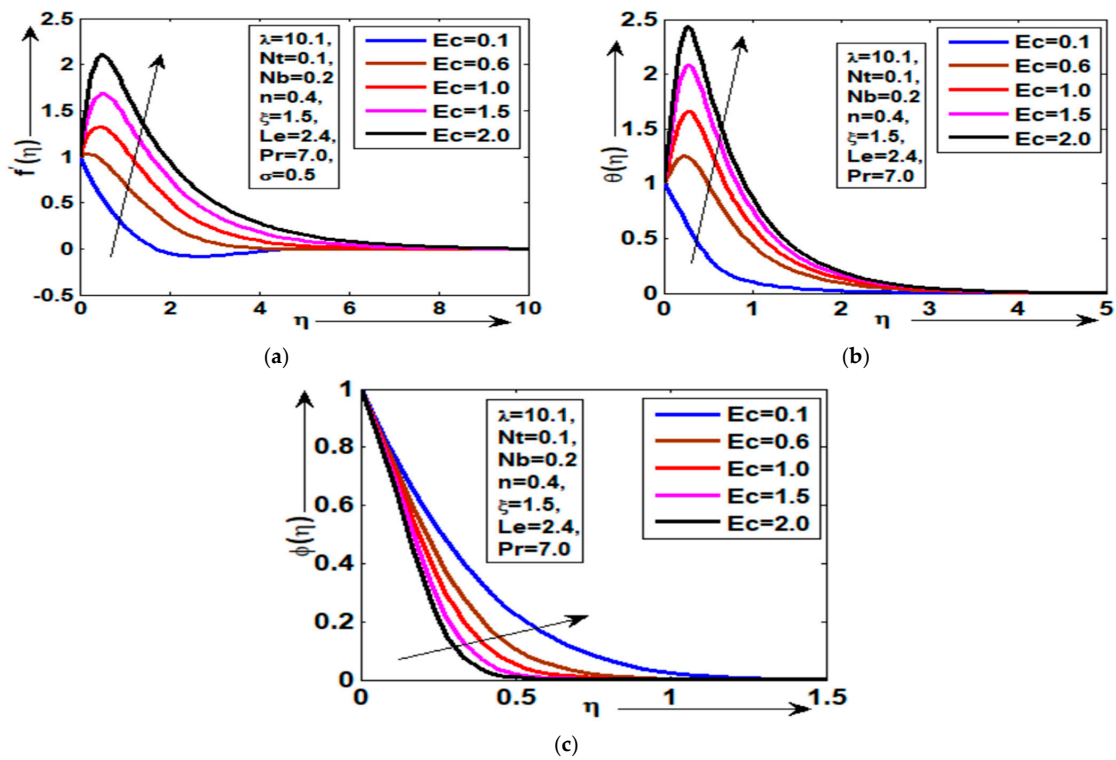


Figure 4. (a–c) Graphical behavior of velocity  $f'(\eta)$ , temperature  $\theta(\eta)$  and concentration  $\phi(\eta)$  for  $Ec$ .

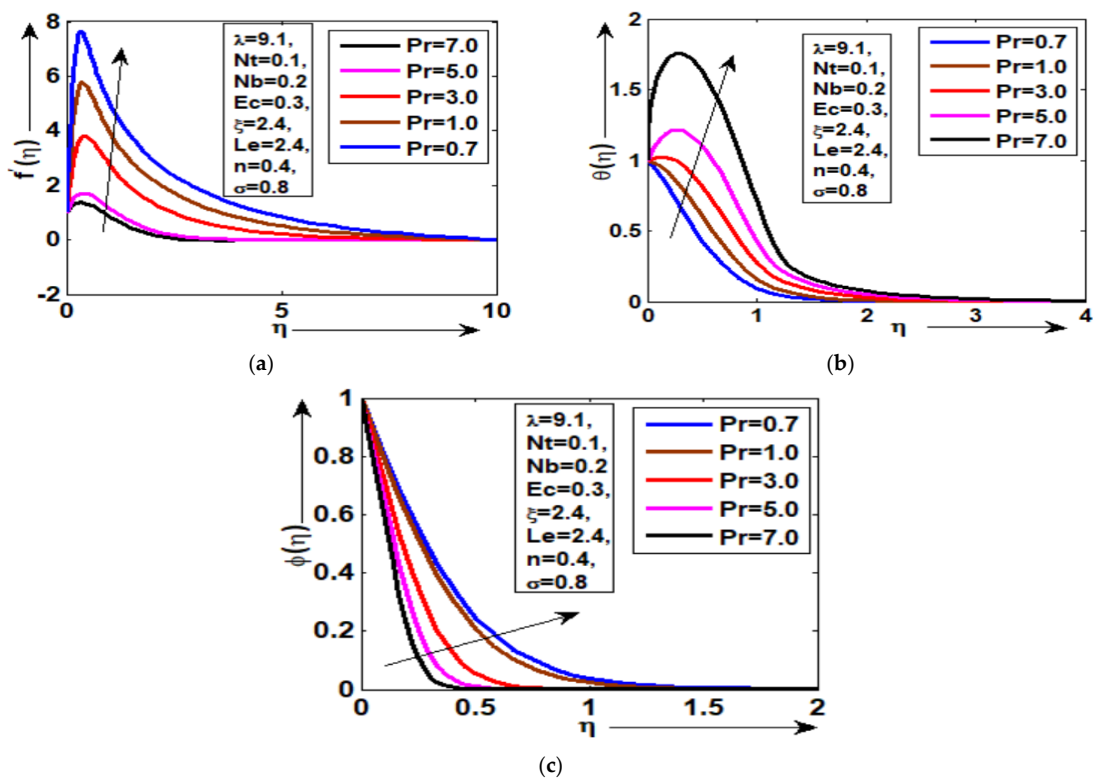


Figure 5. (a–c) Graphical behavior of velocity  $f'(\eta)$ , temperature  $\theta(\eta)$ , and concentration  $\phi(\eta)$  for Pr.

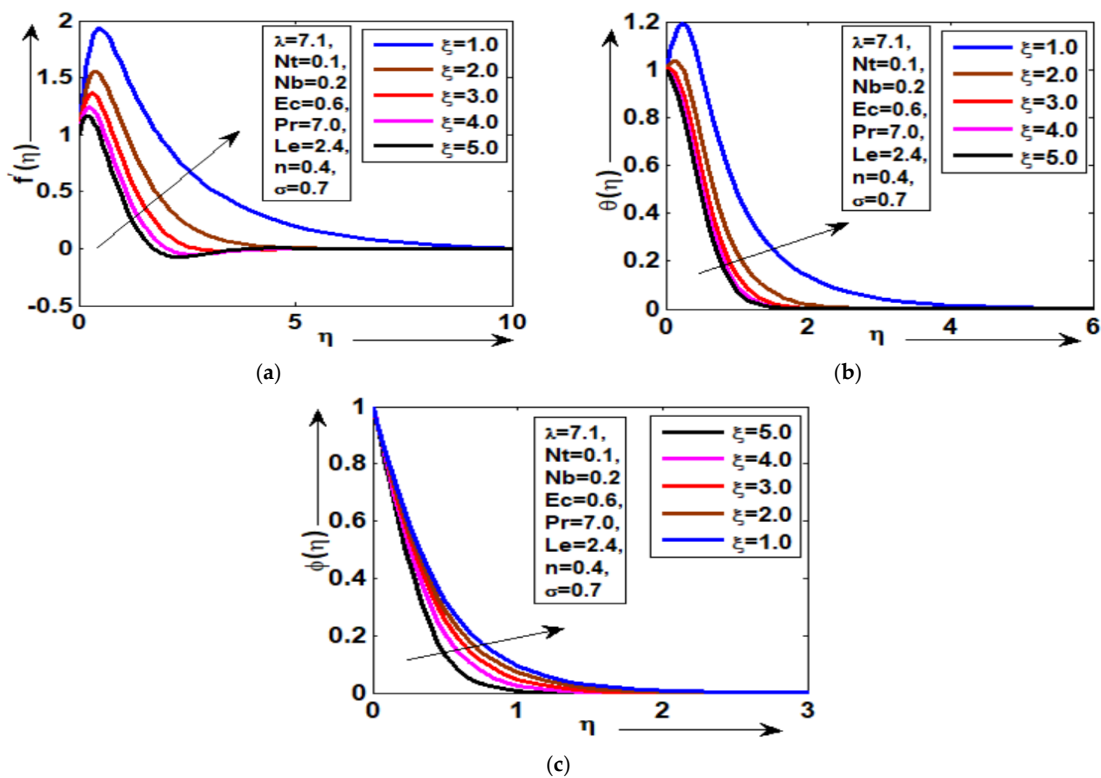


Figure 6. (a–c) Graphical behavior of velocity  $f'(\eta)$ , temperature  $\theta(\eta)$ , and concentration  $\phi(\eta)$  for  $\xi$ .

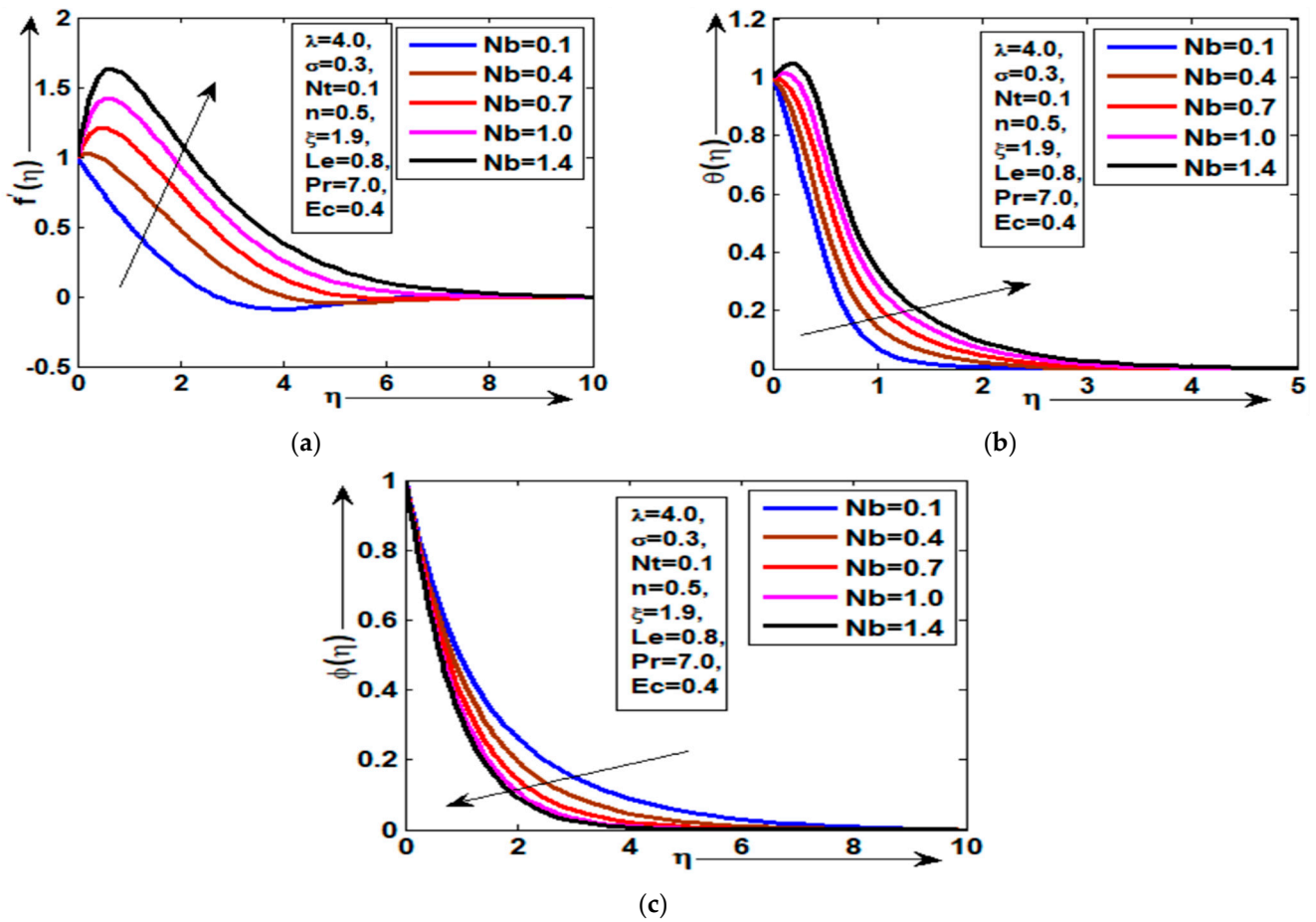


Figure 7. (a–c) Graphical behavior of velocity  $f'(\eta)$ , temperature  $\theta(\eta)$ , and concentration  $\phi(\eta)$  for  $Nb$ .

In addition, the impact of the thermophoretic number  $Nt$  on the physical features of heat and mass transmission across the heated surface is assessed in Figure 8a,b. By increasing  $Nt$ , the heat and mass transfer rates are gradually enhanced with prominent changes in the presence of thermal density and entropy generation. On the other hand, minimum values of  $Nt$  decrease the heat and mass transmission rates with a higher  $Pr$  because the heating conductivity of a liquid with a greater Prandtl quantity is often lesser, which decreases the conductions and improves the amount of heat  $\theta'$  transmission at the surface's interface. In Figure 9a,b, the impact of the Brownian motion parameter  $Nb$  on the mass and heat transmission is evaluated in the presence of thermal density and entropy generation. It can be examined that the dimensionless heat  $\theta'$  transmission declined for the maximum  $Nb$  with  $Pr = 7.0$ . However, the dimensionless mass transfer is increased for the maximum  $Nb$  under buoyant and magnetic attractions. The combination of the density influence and the magnetic attraction serves as a preventing power. The thermal efficiency can be controlled by this preventing power, which has a variety of uses, including the magnetic covering of cables and metallic material and the development of magnetohydrodynamic energy.

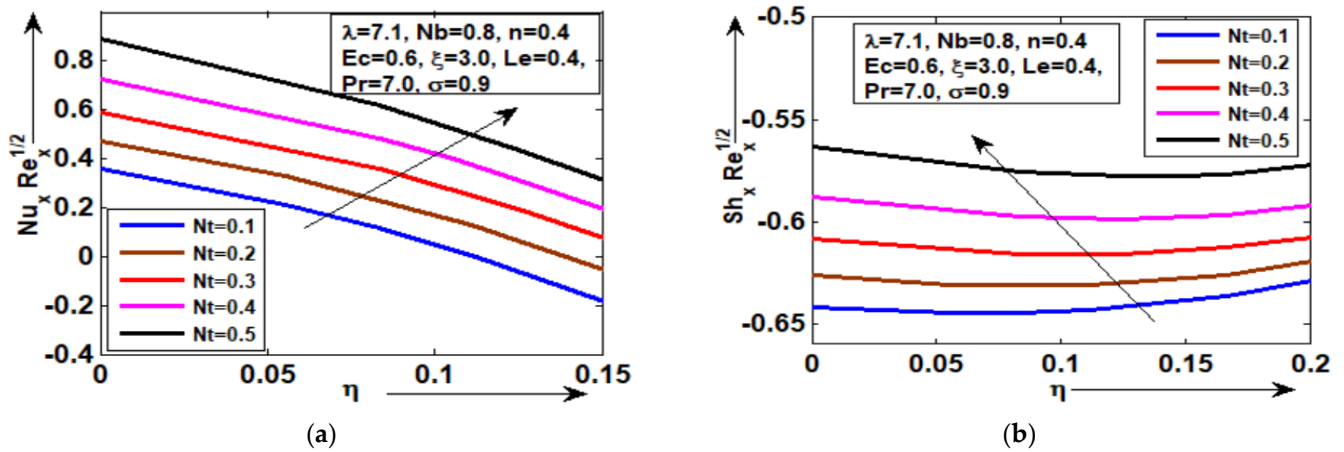


Figure 8. (a,b) Graphical behavior of Nusselt and Sherwood values for  $Nt$ .

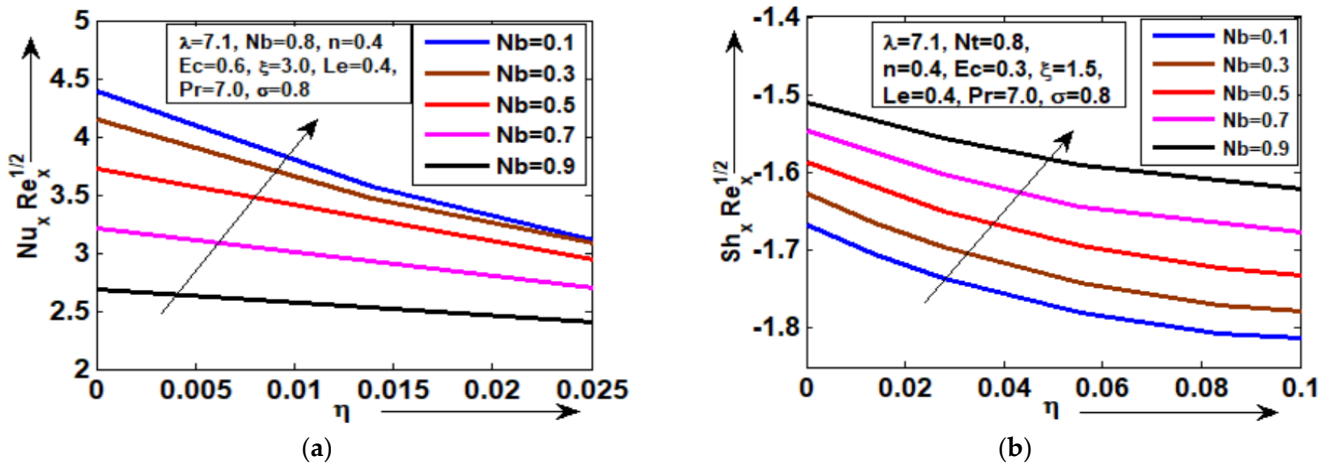


Figure 9. (a,b) Graphical behavior of Nusselt and Sherwood values for  $Nb$ .

In Tables 1 and 2, the computational and numerical calculations of the dimensionless skin friction, heat rate, and mass transfer are computed for diverse factors of the buoyancy parameter  $\lambda$  and the magneto force parameter  $\zeta$  through the stretched surface with temperature–density and entropy effects. The enhancement in friction and Sherwood coefficients is evaluated for the maximum buoyancy  $\lambda = 5.0$ , but the heat transfer is decreased. From a physical standpoint, it was anticipated that the stress variations in the nanofluid nanoparticles would be enhanced by the larger buoyant attraction. The impact of the magneto force  $\zeta$  on the numerical features of heat rate, skin friction, and mass transmission is shown in Table 2. The maximum outcomes of each physical property are determined for higher values of the magneto force. The dimensionless heat and mass rate decreases as the magnetic force decreases. Tables 3 and 4 show the comparable results of the Prandtl number as well as the Lewis variable with the existing works in the literature, including Ibrahim [21], Khan et al. [22], and Dawar et al. [23], with prominent agreement.

Table 1. The computational and numerical calculations for different choices of  $\lambda$ .

$\lambda$	$f'(0)$	$-\theta'(0)$	$-\phi'(0)$
1.0	1.116690859808825	0.917039128307756	0.892601403110183
2.0	0.307505841434577	0.729538072563911	1.122378468495322
3.0	0.484942522867972	0.473890818701673	1.262275440358294
4.0	1.267537306821681	0.186891654885512	1.370478364789618
5.0	2.043499336076714	0.117297572381414	1.462084422804949

**Table 2.** The computational and numerical calculations for different choices of  $\zeta$ .

$\zeta$	$f'(0)$	$-\theta'(0)$	$-\phi'(0)$
0.1	2.183396932316465	1.413888055062002	1.349043083809308
0.3	2.310935199782845	0.603348871052019	1.366341806440679
0.5	2.432294288980072	0.225416928317450	1.383769945241027
0.7	2.547505480184784	1.062897609657398	1.401183250674839
0.9	2.656803884505053	1.901905836106870	1.418483648737034

**Table 3.** The computational and numerical comparisons of  $-\theta'(0)$  for Pr, when  $Nb = Nt = M = Ec = 0$ .

Pr	Ibrahim [21]	Khan et al. [22]	Dawar et al. [23]	Present Results
0.72	0.4636	0.4623	0.4636	0.4617
1.0	0.5822	0.5809	0.5819	0.5811
3.0	1.1652	1.1634	1.1651	1.1645
10.0	2.3080	2.3047	2.3079	2.3071
100.0	7.7657	7.7552	7.7656	7.7639

**Table 4.** The comparison of  $-\phi'(0)$  for several parameters,  $Nt$ ,  $Nb$ ,  $Le$ , and  $\sigma$ .

$Nt$	$Nb$	$Le$	$\sigma$	Dawar et al. [23]	Present Results
0.0				0.967745	0.967631
0.5				0.722754	0.722733
1.0				0.313306	0.313289
	1.0			0.166978	0.166877
	2.0			0.293754	0.293743
	3.0			0.330798	0.330781
		1.0		0.716246	0.716185
		2.0		1.142754	1.142747
		3.0		1.472208	1.472203
			0.1	0.586193	0.586181
			0.2	0.643186	0.643191
			0.3	0.695175	0.695169

## 6. Conclusions

The relationship between the chemical reaction, heat density, and viscous dissipation in a laminar, two-dimensional, mixed convective chemically reactive flow of a magneto nanofluid over a stretching sheet is shown in the present investigation. The fluid density is assumed to be an exponential component of the temperature rather than a linear component as in the Boussinesq model. Because of this, the solution to the issue remains valid across any significant temperature variations, and the outcomes are more precise. The boundary layer equations were developed for the present mechanism under defined boundary conditions. It is important to note that the dimensionless governing mathematical equations were additionally simplified to a group of non-similar calculations with the support of the stream function structure and were numerically incorporated through the Keller box approach to compare the findings with those of previous investigations. The numerical findings obtained from the technique discussed above were geometrically evaluated, and it was discovered that they are in acceptable agreement. The effects of governing flow factors like the Eckert number, density parameter, magnetic force parameter, thermophoretic number, buoyancy number, and Prandtl parameter on the velocity, temperature distribution, and concentration distribution were evaluated prominently via tables and graphs. The prominent key outcomes are described as follows:

- The certain amplitude in the temperature distribution is illustrated as  $n = 0$  but decreases as the density parameter increases. Similarly, the concentration distribution increases as the density of fluid decreases for  $Pr = 7.0$ .

- The temperature of the water-based fluid increases as the Eckert number increases with prominent variations. Physically, it is valid because the entropy generation acts like a heat source to produce the ability in the temperature of the fluid.
- The prominent enhancement in the temperature of the fluid is assessed for the maximum  $Pr$  but decreases as the  $Pr$  decreases. Moreover, the reasonable change in the concentration distribution is evaluated for each  $Pr$  with entropy generation.
- The heat and mass transfer rates are gradually enhanced with a prominent change as  $Nt$  increases under thermal densities and viscous dissipations.
- It is found that the dimensionless Nusselt coefficient is decreased for the maximum  $Nb$  under  $Pr = 7.0$ . However, the dimensionless mass transfer is increased for the maximum  $Nb$  in the presence of buoyancy and magnetic forces.

**Author Contributions:** Conceptualization, Z.U. and A.H.; methodology, Z.U.; software, Z.U.; validation, Z.U.; formal analysis, M.S.A.; investigation, N.H.A.; resources, S.S.; data curation, M.S.A.; writing—original draft preparation, Z.U.; writing—review and editing, Z.U. and A.H.; visualization, S.S.; supervision, Z.U.; project administration, S.S.; funding acquisition, Z.U. and A.H. All authors have read and agreed to the published version of the manuscript.

**Funding:** This research was supported by the Princess Nourah bint Abdulrahman University Researchers Supporting Project (PNURSP2023R259), Princess Nourah bint Abdulrahman University, Riyadh, Saudi Arabia. This work is supported by The University of Lahore under HEC policy.

**Data Availability Statement:** Data sharing is not applicable to this article.

**Acknowledgments:** This research was supported by the Princess Nourah bint Abdulrahman University Researchers Supporting Project (PNURSP2023R259), Princess Nourah bint Abdulrahman University, Riyadh, Saudi Arabia.

**Conflicts of Interest:** The authors declare no conflict of interest.

## Nomenclature

$a$	Constant	$T_\infty$	Ambient temperature
$C$	Nanoparticle volume fraction	$u, v$	Velocity components along $x$ and $y$ axes
$C_w$	Nanoparticle volume fraction at surface	$u_w$	Velocity of the stretching sheet
$C_\infty$	Ambient nanoparticle volume fraction	$x, y$	Cartesian coordinates
$D_B$	Brownian diffusion coefficient		
Greek Symbols			
$D_T$	Thermophoretic diffusion coefficient	$\alpha$	Thermal diffusivity
$f(\eta)$	Dimensionless stream function	$\phi(\eta)$	Rescaled nanoparticle volume fraction
$\kappa$	Thermal conductivity	$\eta$	Similarity variable
$Le$	Lewis number	$\theta(\eta)$	Dimensionless temperature
$N_b$	Brownian motion parameter	$\nu$	Kinematic viscosity of the fluid
$N_t$	Thermophoresis parameter	$\rho_f$	Fluid density
$Nu$	Nusselt number	$\rho_p$	Nanoparticle mass density
$Pr$	Prandtl number	$(\rho c)_f$	Heat capacity of the fluid
$p$	Pressure	$(\rho c)_p$	Heat capacity of nanoparticle material
$q_m$	Wall mass flux	$\tau$	Ratio of heat capacity of nanoparticle and fluid
$q_w$	Wall heat flux	$\psi$	Stream function
$Re_x$	Local Reynolds number	$\lambda$	Buoyancy parameter
$Sh_x$	Local Sherwood number	$\xi$	Magnetic force parameter
$T$	Fluid temperature	$n$	Density parameter
$T_w$	Temperature at the stretching surface	$\sigma$	Reaction rate
$K_c$	Reaction rate constant	$E_c$	Eckert number

## References

1. Khan, M.S.; Karim, I.; Islam, M.S.; Wahiduzzaman, M. MHD boundary layer radiative, heat generating and chemical reacting flow past a wedge moving in a nanofluid. *Nano Converg.* **2014**, *1*, 20. [[CrossRef](#)]
2. Anjum, A.; Masood, S.; Farooq, M.; Rafiq, N.; Malik, M.Y. Investigation of binary chemical reaction in magnetohydrodynamic nanofluid flow with double stratification. *Adv. Mech. Eng.* **2021**, *13*, 16878140211016264. [[CrossRef](#)]
3. Ramya, D.; Raju, R.S.; Rao, J.A. Influence of chemical reaction on MHD boundary layer flow of nanofluids over a nonlinear stretching sheet with thermal radiation. *J. Nanofluids* **2016**, *5*, 880–888. [[CrossRef](#)]
4. Zhang, X.; Li, C.; Zhou, Z.; Liu, B.; Zhang, Y.; Yang, M.; Gao, T.; Liu, M.; Zhang, N.; Said, Z.; et al. Vegetable Oil-Based Nanolubricants in Machining: From Physicochemical Properties to Application. *Chin. J. Mech. Eng.* **2023**, *36*, 76.
5. Kasmani, R.M.; Sivanandam, S.; Bhuvaneshwari, M.; Siri, Z. Effect of chemical reaction on convective heat transfer of boundary layer flow in nanofluid over a wedge with heat generation/absorption and suction. *J. Appl. Fluid Mech.* **2016**, *9*, 379–388. [[CrossRef](#)]
6. Doshi, S.J.; Jain, P.K.; Mehta, N.K. Prospective applications of nano fluid during machining process. *Int. J. Mach. Mach. Mater.* **2013**, *14*, 257–274. [[CrossRef](#)]
7. Jagadha, S.; Gopal, D.; Kishan, N. Nanofluid flow of higher order radiative chemical reaction with effects of melting and viscous dissipation. *J. Phys. Conf. Ser.* **2020**, *1451*, 012003. [[CrossRef](#)]
8. Rao, D.N.; Srikant, R.R.; Krishna, P.V.; Subrahmanyam, M.S. Nano cutting fluids in minimum quantity lubrication. *Proc. Int. Multi-Conf. Eng. Technol. Innov.* **2008**, *1*, 60–63.
9. Afify, A.A. The influence of slip boundary condition on Casson nanofluid flow over a stretching sheet in the presence of viscous dissipation and chemical reaction. *Math. Probl. Eng.* **2017**, *2017*, 3804751. [[CrossRef](#)]
10. Hasin, F.; Ahmad, Z.; Ali, F.; Khan, N.; Khan, I.; Eldin, S.M. Impact of nanoparticles on vegetable oil as a cutting fluid with fractional ramped analysis. *Sci. Rep.* **2023**, *13*, 7140. [[CrossRef](#)]
11. Srikant, R.; Prasad, M.; Amrita, M.; Sitaramaraju, A.; Krishna, P.V. Nanofluids as a potential solution for minimum quantity lubrication: A review. *Proc. Inst. Mech. Eng. Part B J. Eng. Manuf.* **2013**, *228*, 3–20. [[CrossRef](#)]
12. Kadirgama, K. Nanofluid as an alternative coolant in machining: A review. *J. Adv. Res. Fluid Mech. Therm. Sci.* **2021**, *69*, 163–173. [[CrossRef](#)]
13. Li, C.; Ali, H.M. Enhanced Heat Transfer Mechanism of Nanofluids Minimum Lubrication Grinding. In *Research Anthology on Synthesis, Characterization, and Applications of Nanomaterials*; IGI Global: Hershey, PA, USA, 2021; pp. 928–950. [[CrossRef](#)]
14. Sharma, A.K.; Tiwari, A.K.; Dixit, A.R. Progress of nanofluid application in machining: A review. *Mater. Manuf. Process.* **2014**, *30*, 813–828. [[CrossRef](#)]
15. Chakule, R.R.; Chaudhari, S.S.; Chandratre, K.V.; Patole, P.B.; Talmale, P.S. Nanofluids, micro-lubrications and machining process optimisations—A review. *Manuf. Rev.* **2023**, *10*, 1. [[CrossRef](#)]
16. Rifat, M.; Rahman, H.; Das, D. A review on application of nanofluid MQL in machining. *AIP Conf. Proc.* **2017**, *1919*, 020015. [[CrossRef](#)]
17. Sidik, N.A.C.; Samion, S.; Ghaderian, J.; Yazid, M.N.A.W.M. Recent progress on the application of nanofluids in minimum quantity lubrication machining: A review. *Int. J. Heat Mass Transf.* **2017**, *108*, 79–89. [[CrossRef](#)]
18. Amin, A.R.; Ali, A.; Ali, H.M. Application of Nanofluids for Machining Processes: A Comprehensive Review. *Nanomaterials* **2022**, *12*, 4214. [[CrossRef](#)]
19. Pasam, V.K.; Rapeti, P.; Battula, S.B. Efficacy of Nanocutting Fluids in Machining—An Experimental Investigation. *Adv. Technol. Innov.* **2018**, *3*, 78.
20. Lautenschlaeger, M.P.; Stephan, S.; Horsch, M.T.; Kirsch, B.; Aurich, J.C.; Hasse, H. Effects of lubrication on friction and heat transfer in machining processes on the nanoscale: A molecular dynamics approach. *Procedia CIRP* **2018**, *67*, 296–301. [[CrossRef](#)]
21. Ibrahim, W. MHD boundary layer flow and heat transfer of micropolar fluid past a stretching sheet with second order slip. *J. Braz. Soc. Mech. Sci. Eng.* **2017**, *39*, 791–799. [[CrossRef](#)]
22. Khan, R.M.; Ashraf, W.; Sohail, M.; Yao, S.-W.; Al-Kouz, W. On behavioral response of microstructural slip on the development of magnetohydrodynamic micropolar boundary layer flow. *Complexity* **2020**, *2020*, 8885749. [[CrossRef](#)]
23. Dawar, A.; Shah, Z.; Tassaddiq, A.; Islam, S.; Kumam, P. Joule heating in magnetohydrodynamic micropolar boundary layer flow past a stretching sheet with chemical reaction and microstructural slip. *Case Stud. Therm. Eng.* **2021**, *25*, 100870. [[CrossRef](#)]
24. Salem, A.M.; El-Aziz, M.A.; Abo-Eldahab, E.M.; Abd-Elfatah, I. Effect of variable density on hydromagnetic mixed convection flow of a non-Newtonian fluid past a moving vertical plate. *Commun. Nonlinear Sci. Numer. Simul.* **2010**, *15*, 1485–1493. [[CrossRef](#)]
25. Siddiqua, S.; Asghar, S.; Hossain, M.A. Radiation effects in mixed convection flow of a viscous fluid having temperature-dependent density along a permeable vertical plate. *J. Eng. Phys. Thermophys.* **2012**, *85*, 339–348. [[CrossRef](#)]
26. Siddiqua, S.; Hossain, M.A.; Gorla, R.S.R. Temperature-dependent density effect on natural convection flow over a horizontal circular disk. *J. Thermophys. Heat Transf.* **2016**, *30*, 890–896. [[CrossRef](#)]
27. Elkaroui, A.; Amamou, A.; Ben Khalifa, R.; Said, N.M.; Gazzah, M.H.; El-Rahman, M.A. Numerical predictions of near field behavior of variable density non-reacting turbulent round jets. *Int. J. Heat Mass Transf.* **2020**, *160*, 120201. [[CrossRef](#)]
28. Ullah, Z.; Aldhabani, M.S. Physical Analysis of Thermophoresis and Variable Density Effects on Heat Transfer Assessment along a Porous Stretching Sheet and Their Applications in Nanofluid Lubrication. *Lubricants* **2023**, *11*, 172. [[CrossRef](#)]

29. Cossali, G.E.; Tonini, S. Modelling the effect of variable density and diffusion coefficient on heat and mass transfer from a single component spherical drop evaporating in high temperature air streams. *Int. J. Heat Mass Transf.* **2018**, *118*, 628–636. [[CrossRef](#)]
30. Laaroussi, N.; Lauriat, G.; Desrayaud, G. Effects of variable density for film evaporation on laminar mixed convection in a vertical channel. *Int. J. Heat Mass Transf.* **2009**, *52*, 151–164. [[CrossRef](#)]
31. Ashraf, M.; Ullah, Z. Effects of variable density on oscillatory flow around a non-conducting horizontal circular cylinder. *AIP Adv.* **2020**, *10*, 015020. [[CrossRef](#)]
32. Sanders, J.P.H.; Sarh, B.; Gökalp, I. Variable density effects in axisymmetric isothermal turbulent jets: A comparison between a first-and a second-order turbulence model. *Int. J. Heat Mass Transf.* **1997**, *40*, 823–842. [[CrossRef](#)]
33. Han, Z.; Reitz, R.D. A temperature wall function formulation for variable-density turbulent flows with application to engine convective heat transfer modeling. *Int. J. Heat Mass Transf.* **1997**, *40*, 613–625. [[CrossRef](#)]
34. Yoo, G.; So, R. Variable density effects on axisymmetric sudden-expansion flows. *Int. J. Heat Mass Transf.* **1989**, *32*, 105–120. [[CrossRef](#)]
35. Prabhu, S.V.; Mahulikar, S.P. Effects of density and thermal conductivity variations on entropy generation in gas micro-flows. *Int. J. Heat Mass Transf.* **2014**, *79*, 472–485. [[CrossRef](#)]
36. Yeranee, K.; Rao, Y.; Yang, L.; Li, H. Enhanced thermal performance of a pin-fin cooling channel for gas turbine blade by density-based topology optimization. *Int. J. Therm. Sci.* **2022**, *181*, 107783. [[CrossRef](#)]
37. Yan, H.-N.; Liu, C.-L.; Zhang, L.; Bai, X.-H.; Zhang, F. Effects of viscosity and density on film cooling effectiveness of turbine blade with pressure gradient and surface curvature. *Int. J. Therm. Sci.* **2023**, *193*, 108517. [[CrossRef](#)]
38. Ullah, Z.; Akkurt, N.; Alrihieli, H.F.; Eldin, S.M.; Alqahtani, A.M.; Hussanan, A.; Ashraf, M.; Jabeen, M. Temperature-Dependent Density and Magnetohydrodynamic Effects on Mixed Convective Heat Transfer along Magnetized Heated Plate in Thermally Stratified Medium Using Keller Box Simulation. *Appl. Sci.* **2022**, *12*, 11461. [[CrossRef](#)]
39. Ullah, Z.; El-Zahar, E.; Aldhabani, M.S.; Alrihieli, H.F.; Seddek, L.F. Heat transfer assessment with entropy generation and thermal density effects on boundary layer flow of magneto nanofluid across the stretching sheet under magnetic field. *Therm. Sci. Eng. Prog.* **2023**, *43*, 101955. [[CrossRef](#)]
40. Gamaoun, F.; Ullah, Z.; Ahammad, N.A.; Fadhl, B.M.; Makhdoum, B.M.; Khan, A.A. Effects of thermal radiation and variable density of nanofluid heat transfer along a stretching sheet by using Keller Box approach under magnetic field. *Therm. Sci. Eng. Prog.* **2023**, *41*, 101815. [[CrossRef](#)]
41. Dolatabadi, N.; Rahmani, R.; Rahnejat, H.; Garner, C.P.; Brunton, C. Performance of poly alpha olefin nanolubricant. *Lubricants* **2020**, *8*, 17. [[CrossRef](#)]

**Disclaimer/Publisher’s Note:** The statements, opinions and data contained in all publications are solely those of the individual author(s) and contributor(s) and not of MDPI and/or the editor(s). MDPI and/or the editor(s) disclaim responsibility for any injury to people or property resulting from any ideas, methods, instructions or products referred to in the content.